Nanoscale Horizons

ROYAL SOCIETY OF CHEMISTRY

COMMUNICATION

View Article Online
View Journal | View Issue

Cite this: *Nanoscale Horiz.*, 2025, 10, 2411

Received 30th April 2025,
Accepted 9th July 2025

DOI: 10.1039/d5nh00295h

rsc.li/nanoscale-horizons

"Cell climbing stones" – varying the surfaces of electrospun nanofibers with protrusions as secondary structures to manipulate neural cell behaviors†

Yawen Wang,[ab] Xiaopei Zhang,[ac] Lijie Yao,[a] Yuying Yan,[a] Yuanfei Wang [d] and Tong Wu *[ac]

Effective neural repair requires the precise regulation of neurite outgrowth and coordinated migration of neural stem cells (NSCs) and Schwann cells (SCs). The synergistic integration of topographical cues, chemical signals and electrical stimulation can significantly enhance this process, among which topographical modulation has emerged as a research focus due to its direct regulatory effects on cellular behavior. Micro/nanoscale topological features (nanogrooves and protrusions) can markedly promote neurite outgrowth and cell migration by matching the mechanical characteristics of growth cone filopodia (100–300 nm). Building upon our previous work, we designed a series of aligned nanofibers with SiO_2 protrusions of varying sizes and concentrations to mimic "cell climbing stones," systematically investigating their regulatory effects on neurite growth, and the migration of NSCs and SCs. The results demonstrated that nanofibers with oriented protrusions as secondary structures significantly enhanced the motility of SCs and NSCs while promoting neurite extension. Notably, nanofibers fabricated with 200 nm SiO_2 nanoparticles blended with PCL at 6% SiO_2 concentration exhibited the most pronounced regulatory effects on neural cell behavior.

New concepts

We innovatively developed an aligned nanofiber scaffold with bioinspired surface topological structures. By integrating electrospinning technology with the tunable self-assembly of silica nanoparticles, we successfully constructed nanoscale protrusions mimicking the texture of "climbing stones" on the fiber surfaces as a secondary structure. This scaffold effectively provides the necessary "footholds" conducive to the growth and migration of nerve cells. Unlike conventional nerve guidance scaffolds relying solely on fiber alignment, this design represents the first realization of synergistic regulation between macroscopic fiber orientation and surface nanotopography. Through systematic optimization of preparation parameters, we achieved a three-dimensional microenvironment with precisely controlled surface morphological characteristics. Experimental results demonstrated that this multiscale architecture could significantly enhance the migration of Schwann cells and neural stem cells and facilitate neurite outgrowth. The research elucidates the mechanism by which surface nanotopographical features influence neural cell behavior and establishes a controllable fabrication method for bioinspired hierarchical scaffolds. These findings not only provide novel design principles for neural regeneration materials but also deepen our understanding of cell–nanomaterial interactions, with significant scientific value.

1. Introduction

During the repair and regeneration processes following neural injuries, the growth and extension of neurites and the migration of neural stem cells (NSCs) along with glial cells are pivotal to neural regeneration. The comprehensive design of neural conduits or biomimetic scaffolds incorporating features, such as topographical cues, chemical signals, electrical stimulation, and their synergistic combinations is essential to enhance the growth and elongation of neurites as well as the efficient migration of these related cells.[1–4] Among them, the application of topographical cues has become a focus of attention, as these can substantially influence the behavior of nerve cells through direct interaction with the underlying materials at both the cellular and subcellular levels.

As a result, in recent years, a plethora of research endeavors have been directed towards elucidating the intricate relationship between topographical guides and cellular behavior.

[a] *Medical Research Center, The Affiliated Hospital of Qingdao University, Qingdao University, Qingdao 266000, China. E-mail: twu@qdu.edu.cn*
[b] *School of Rehabilitation Sciences and Engineering, University of Health and Rehabilitation Sciences, Qingdao 266113, China*
[c] *Shandong Key Laboratory of Medical and Health Textile Materials, Collaborative Innovation Center for Eco-textiles of Shandong Province and the Ministry of Education, College of Textile & Clothing, Qingdao University, Qingdao 266071, China*
[d] *Qingdao Stomatological Hospital Affiliated to Qingdao University, Qingdao 266001, China*

† Electronic supplementary information (ESI) available. See DOI: https://doi.org/10.1039/d5nh00295h

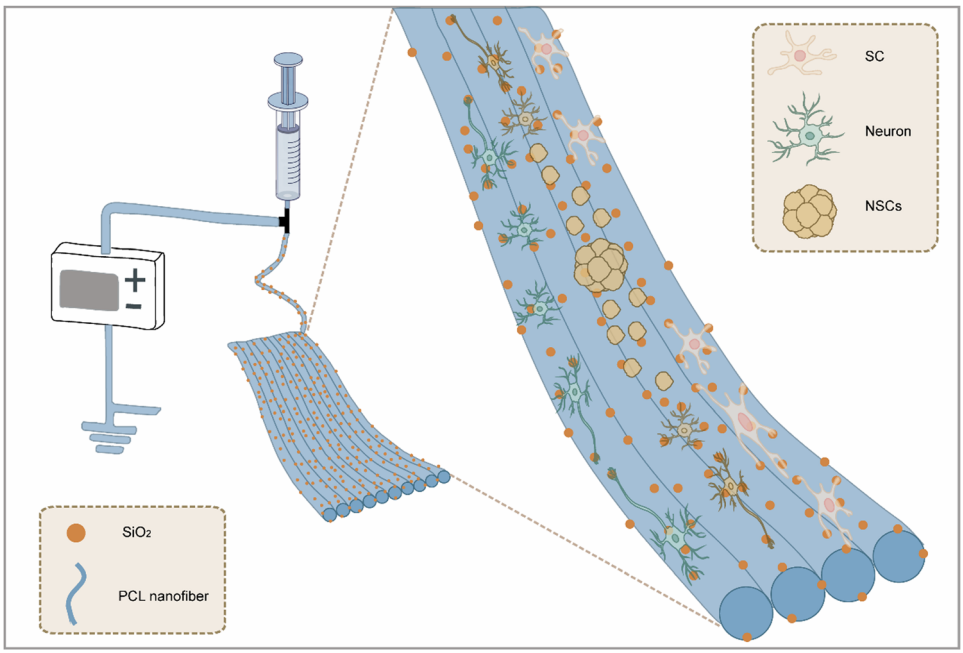

Scheme 1 Schematic illustration showing the regulatory effects of "cell climbing stones" on neurite outgrowth and the migration of NSCs and SCs.

Experimental findings garnered through these studies have consistently demonstrated that a spectrum of characteristic material attributes potently modulate the performance of neurons *in vitro*. Notably, these include surface roughness, which has been found to impact neuronal adhesion measurably, viability as described by the nuances of substrate susceptibility,[5,6] axonal orientation as articulated by precise alignment patterns,[7,8] and the proliferation of neurites.[9] These seminal observations underscore the role of topographical cues as pivotal mediators of neuronal interactions with the extracellular milieu. Moreover, the spatial arrangement and density of nanofibers,[10] the microscale roughness or gradients in density attributed to particles from electrospraying,[4,11] as well as the sub-micron irregular patterns generated from materials such as graphene oxide,[12–14] can all significantly modulate the behavior of nerve cells to varying extents. Topographical guidance is particularly significant in the design of materials for neural regeneration, offering valuable biological standards to enhance the performance of the materials. From the perspective of materials engineering, we should appropriately adjust the characteristics and topological structure of the material surface to achieve the optimal effect of guiding cell growth and movement, ultimately promoting efficient nerve regeneration.

In an array of topographical features, nanoscale features, such as protrusions, arrays of bulges and groove designs, are deemed most effective for guiding and elongating neurites. These nanodimensional details furnish growth cones, the exploratory structures at the forefront of neurite growth, with ample sensory cues and suitable zones for engagement, critically facilitating neuronal development in various substrates.[15–17] Specifically, established studies have shown that surfaces patterned with nanoscale grooves can significantly promote the elongation of neurites. For example, upon the integration of nanoscale grooves into the surface of electrospinning nanofibers, a notable enhancement in the outgrowth of neurites derived from the dorsal root ganglion (DRG) of chickens has been observed.[18] These studies point to the importance of micro- and nano-structured topographies providing highly precise mechanical guidance for neurite growth, thereby facilitating the process of neural regeneration and repair.

Aligned electrospinning nanofibers with nanoscale protrusions on the surface have been demonstrated to effectively promote the extension of neurites and the migration of NSCs. This phenomenon can be intuitively grasped through an analogy with the process of rock climbing. Analogously, a smooth wall

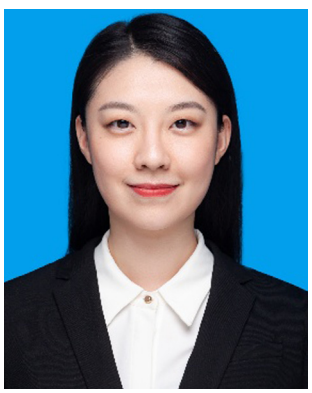

Tong Wu

Tong Wu has served as an Early Career Community Board Member for Nanoscale Horizons since 2020. She was also awarded the Emerging Investigator and Women in Nanoscience collection by the RSC journals in 2023. She is very honored and happy to have grown with the journal over the past five years. She is very excited to contribute this article for the development of bio-inspired nanostructures and their exploration for biomedical applications. She sincerely congratulates Nanoscale Horizons on its 10th anniversary and wishes the journal continued success and a wonderful future.

poses a challenge to climbers, as it lacks essential handholds and footholds. In contrast, when protrusions strategically placed and dimensioned to match the width of a climber's hand and feet, they significantly ease the ascent. By fine-tuning the calibration of these features, akin to matching the grip size and span to the climber's physical attributes, the efficiency and velocity of climbing are notably augmented. This approach not only eases the climb but also serves to amplify the overall performance during the ascent. In the process of neuronal regeneration, neural cells effectively act as climbers, with electrospinning nanofibers serving as the climbing wall. The meticulous modulation of the size and interval of nanoscale silica (SiO_2) protrusions on the surface of these electrospinning nanofibers allows them to align with the biomechanical properties and contact requirements of specific types of cells (Scheme 1). This delicate system of biophysical interfacing facilitates the directed outgrowth of neurites and migration of nerve cells, thereby suggesting the strategic use of micro- and nano-structured nanofibers as a critical means for enhancing reparative neural processes.

For example, the processes of neurite outgrowth and path selection during neurodevelopment are crucially influenced by the organization of actin-based cytoskeletal elements such as microfilaments. These proteinaceous constituents, termed filopodia and lamellipodia, essentially serve as guiding cues during developmental stages, with diameters typically ranging from 100 to 300 nm. Such structural components are essential for the directed growth and navigational precision of neurites.[19] Consequently, the most potent substrates to advance neurite outgrowth should emulate the dimensional heterogeneity of the extracellular matrix, thereby aiming to enhance the efficiency of neural guidance. Precisely controlling microscale surface characteristics on electrospun fiber matrices, notably by incorporating topographical patterns at 1 μm and 200 nm, aligns with the dimensions of axons that participate in swift neural conduction as well as the dimensions of filopodia in growth cones, thus optimizing neural navigation.[20] We speculate that the presence of nanoscale protrusions on the surfaces of electrospinning nanofibers could play a crucial role in facilitating neurite outgrowth and migration of neural cells. This innovative design conceptualizes the fibers as nanoscale climbing frameworks, enhancing the interactions between neural cells and the substrate, effectively offering a high-fidelity approximation of their natural "cell climbing stones."

In this study, leveraging existing research,[21] we have systematically designed and fabricated a series of uniaxially aligned

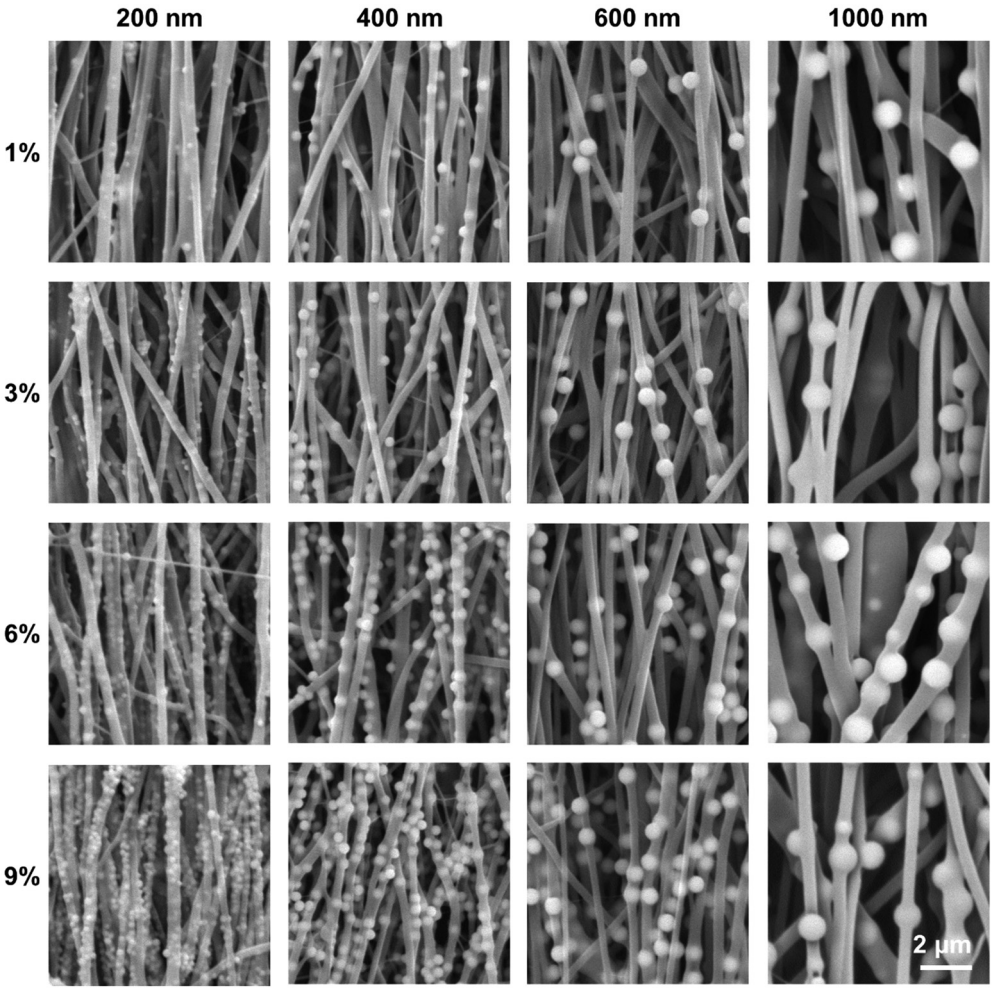

Fig. 1 SEM images of the different PCL/SiO_2 hybrid nanofibers. The SiO_2 protrusions on the fiber surfaces were defined as the "cell climbing stones".

electrospinning nanofibers with surfaces endowed with SiO_2 protrusions, engineered in various dimensions and concentrations. We have rigorously examined and substantiated their modulatory impacts on the directional outgrowth of neurites, as well as the migration of both NSCs and Schwann cells (SCs), to underscore their potential applications in neural tissue engineering and regeneration strategies.

2. Results and discussion

This research first achieved the successful preparation of SiO_2 nanoparticles with diameters of 200 nm, 400 nm, 600 nm, and 1000 nm using the Stöber method. These nanoparticles were then combined with the biocompatible polymer poly(ε-caprolactone) (PCL) and used as the matrix material in an electrospinning process to produce nanofibers with distinct surface protrusions exhibiting varying dimensions and concentrations of SiO_2. Fig. 1 displays the scanning electron microscopy (SEM) images of PCL/SiO_2 hybrid aligned nanofibers, which exhibit protrusions of varying diameters and concentrations on the surface. It can clearly be seen from the images that the SiO_2 particles are successfully dispersed throughout the nanofibers, resulting in the formation of surface protrusions as secondary structures with different sizes and concentrations, regardless of the diameter of the SiO_2 particles. At an SiO_2 concentration of 9%, the distribution of the protrusions on the fiber surface becomes exceptionally dense. The particle density of SiO_2 detailed in Fig. S1 (ESI†).

Furthermore, in contrast to isolated protrusion structures, 600 nm diameter SiO_2 particles establish a continuous ''bead necklace''-like structure in association with the fiber matrix. The diameters of all hybrid nanofiber samples fell within the range of 360 nm to 460 nm, with consistent uniformity in fiber thickness. The average diameters of the different fiber groups, along with their normal distribution, are depicted in Fig. S2 (ESI†). For protrusions exhibiting a diameter of 200 nm, an increase in the concentration of SiO_2 was accompanied by an expansion in the diameter of the nanofibers. This phenomenon can be attributed to the relatively small size of the 200 nm protrusions, which are significantly smaller than the diameter of the electrospinning nanofibers. As the SiO_2 concentration rises, the accumulation of SiO_2 within the fibers increases, resulting in an increase in fiber diameter due to the added structural support. For SiO_2 particles with diameters of 400 nm and 600 nm, the fiber diameter exhibited an absence of a discernible trend in response to increasing concentration. Notably, within the 400 nm particle group, there was a relatively low variance in fiber diameter across different concentrations. This observation is attributed to the similarity in size between the 400 nm SiO_2 particles and the electrospinning nanofibers, as a result, with the rise in concentration, the particles do not accumulate excessively, resulting in only slight alterations to the fiber diameter. For SiO_2 particles with a diameter of 600 nm, as the particle size exceeds that of the nanofibers, as the concentration increases, the SiO_2 particles exert varying degrees of ''tugging'' on the electrospinning nanofibers, leading to the nanofibers being progressively drawn into finer diameters. Therefore, the change in diameter does not exhibit a regular pattern across different concentrations of SiO_2 particles. The scanning SEM images and the normal distribution plot of fiber diameter for pure PCL nanofibers, synthesized under identical spinning parameters, are presented in Fig. S3 (ESI†). The fibers displayed a consistent and uniform thickness, and upon comparison with the fibers containing SiO_2 particles, the diameter of the PCL fibers was maintained within a range of 360 nm to 460 nm.

Speaking of ''bead necklace''-like structure, one study demonstrates the successful directional alignment of SiO_2 particles through the optimization of solution composition and electrospinning parameters. Initially, the researchers controlled solution viscosity by adjusting the polyvinyl alcohol (PVA)/SiO_2/H_2O ratio to an optimal weight ratio of 7 : 19 : 75, which was effective in optimizing chain entanglement and mitigating particle aggregation. Subsequently, the particle size was selectively filtered, revealing that particles exceeding 265 nm were more prone to form necklace-like structures, while particles with a diameter of 143 nm, due to their higher surface energy, were more susceptible to agglomeration and less amenable to directional arrangement. Ultimately, the study identified the optimal voltage range for electrospinning to be between 10 and 20 kV, as voltages exceeding this range were associated with the formation of berry-like defects.[22]

In response to the observed uneven distribution of SiO_2 particles on the fibers in our study, we have referred to the methods described in the aforementioned literature and proposed the following improvement strategies: improving the solvent system by using a low-boiling-point co-solvent to replace HFIP, which accelerates polymer solidification during electrospinning and fixes the position of the particles,[11] and surface-modification of the SiO_2 particles by introducing amino silane coupling agents to enhance the compatibility between the particles and the polymer, thereby inhibiting particle migration and aggregation.

Analysis of the SEM images presented in Fig. 1 indicates that the 1000 nm group does not conform to the expected ''climbing stone'' morphology but adopts a ''huge pearl necklace'' configuration. Furthermore, from the SEM images, there was no discernible variation in the fiber morphology and the spacing between the SiO_2 particles across different concentration levels. As a result, we did not include the 1000 nm group into our study. Instead, our focus was redirected to the biological significance of particles within the 200–600 nm size range, which is more pertinent to our research objectives.

The migration of SCs plays a crucial role in neuroregenerative and reparative processes.[23,24] Consequently, we hypothesize that the ''cell climbing stone'' intended for the development of neural regeneration scaffolds may exert control over SCs migration. To this end, we first investigated the regulatory effects of the ''cell climbing stone'' with the aforementioned different parameters on the linear migration of SCs. SCs were seeded onto the left-hand side of a 0.5 mm wide area of a dimethylsiloxane block, in

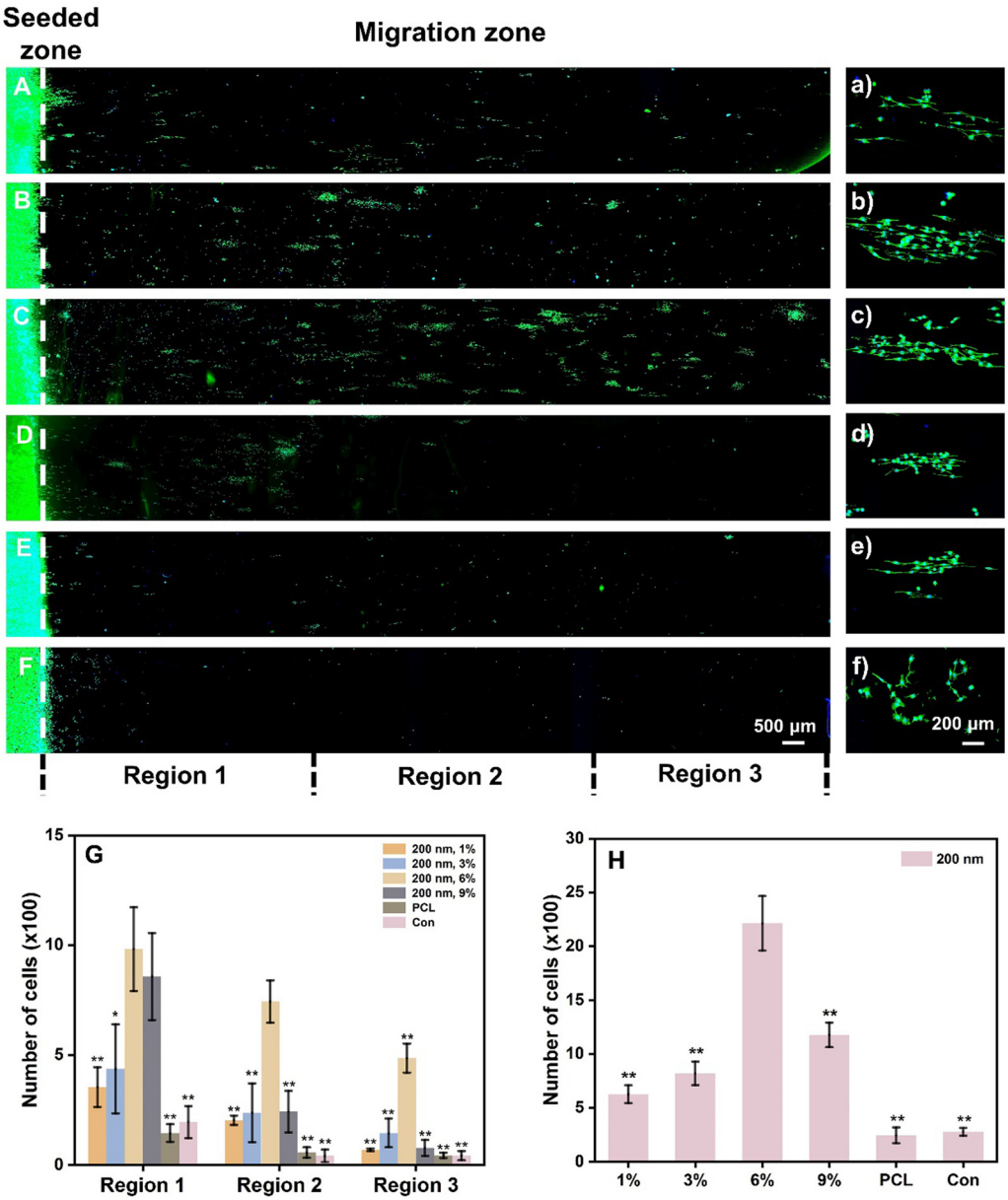

Fig. 2 Fluorescence images of the migration of SCs on the different fibers after culture for 3 days: (A) group 200 nm, 1%; (B) group 200 nm, 3%; (C) group 200 nm, 6%; (D) group 200 nm, 9%; (E) group PCL; (F) group Con. The magnified images in (a)–(f) show the morphologies of SCs in the migration zone. Green: Phalloidin-iFluor 488; Blue: DAPI. (G) The number of SCs in the different migration zones of group 200 nm; (H) statistics of total migrated SCs of group 200 nm. $*P < 0.05$, $**P < 0.01$, and $***P < 0.001$ as compared with group 200 nm, 6%.

contact with PCL/SiO_2 hybrid fibers with different parameter settings. Following cell adhesion, the polydimethylsiloxane block was removed to facilitate the migration of the cells towards the right-hand side. The migration outcomes are depicted in Fig. 2, where Scheme 1 provides a schematic illustration of SCs migration across the various ''stone-climbing'' substrates with distinct parameters. Fig. 2A–F show fluorescence images of SCs migrating on ''climbing stone'' substrates with spike diameters of 200 nm and Fig. 2(a)–(f) show their cell morphology. Due to the guidance provided by the contact with oriented nanofibers, SCs migrate along the direction of uniaxial alignment. We then assessed the migration of SCs by measuring the number of cells in the migration region, which was divided into three distinct areas. With observations solely from the fluorescence images, the migration of SCs on ''climbing stone'' substrates featuring nanoscale protrusions (Fig. 2A–D) exhibited a more significant migration response compared to those on smooth pure PCL nanofibers (Fig. 2E) or the control (Con) group (Fig. 2F).

Specifically, within the range of 200 nm diameter ''climbing stone'' substrates, the SCs demonstrated the most pronounced migratory efficacy at an SiO_2 concentration of 6%. Statistical analysis of the number of SCs migrating across different regions, along with the total cell count in the migration zones, is illustrated in Fig. 2G and H. The results reveal that the ''cell

climbing stone'' group, characterized by nanoscale protrusions, exhibited a significantly higher number of cells in all migration areas compared to the smooth pure PCL group and the Con group. Moreover, the total number of migrating cells in the ''cell climbing stone'' groups was appreciably greater than that in either the PCL or Con groups, with statistically significant differences. These findings suggest that nanoscale protrusions on the surface of oriented nanofibers are capable of effectively enhancing the migration of SCs. Additionally, our analysis indicates that within a single sample, there is variability in the number of cellular migrations across different migration zones. SCs initiate their migration process uniformly from the ''seed region,'' with the collective migration dynamics predominantly driven by the locomotion of leading cells and the interactions between these leading cells and their trailing companions.[25] Given the intrinsic and inter-individual variability in cellular motility, the geometric shapes of cell clusters or monolayers are expected to vary widely. This diversity is expected to contribute to the heterogeneity observed in cell–cell collisions and adhesion events. Furthermore, the availability of adjacent free locations within the vicinity plays a significant role in modulating the migratory potential of the cells. Generally, the inability of cell clusters to migrate cohesively as a unified entity results in inconsistent cell densities across different migration zones.

In the experimental setup of the ''cell climbing stone'' with different parameters, the 200 nm, 6% treatment group consistently exhibited the most numerous cell counts across all areas of cell migration, along with the greatest total number of migrating cells. Statistical comparisons with the other treatment groups revealed significant disparities in these parameters. The migration behavior of SCs on nanofibers with diameters of 400 nm and 600 nm, decorated with SiO_2 protrusions at different concentrations, is illustrated in Fig. S4 and S5 (ESI†). Notably, the SCs exhibited enhanced migration performance on all nanofibers featuring surface protrusions, with both the overall migration rate and the migration counts across individual regions significantly outperforming those observed on pure PCL and Con samples. Within the 400 nm group, SCs predominantly localized to region 1, with the 400 nm 6% subgroup demonstrating the highest number of cell migrations. In region 2, no statistically significant differences were observed in the cell counts among the various groups. Similarly, in region 3, no significant differences in cell counts were detected among all groups, excluding the Con group. Overall, the 400 nm 6% subgroup exhibited the most effective cell migration, as evidenced by the highest cumulative migration counts. In the 600 nm group, statistical analysis of cell numbers across various regions (Fig. S5C, ESI†) indicated that region 1 contained the highest cell density. Within region 1, no significant differences were observed between the different dendritic groups. However, there were statistically significant differences in region 1 compared to the pure PCL group and the Con group. In region 2, the 600 nm 3% group exhibited the most favorable performance, although it did not differ significantly from the 600 nm 9% group. Similar to region 1, region 3 showed no significant differences in cell counts except between the PCL and Con groups. With respect to total migration, both the 600 nm 3% and 600 nm 9% groups demonstrated the most effective migration outcomes.

In the realm of characterizing cellular migration, contemporary research has utilized more sophisticated and precise analytical techniques. In the current study, following cell seeding on a designated surface, the cells were cultivated within an incubation chamber integrated into a live-cell workstation. The temperature and atmospheric conditions within this incubation chamber were meticulously adjusted to be identical to those of a conventional cell culture incubator. The cells were subjected to live-cell time-lapse imaging using an inverted fluorescence microscope system equipped with a charge-coupled device (CCD). This advanced equipment and methodology enable clear delineation of cellular migration trajectories and individual cell paths, providing more intuitive insights into cell behavior.[26] Acknowledging the limitations of the available equipment and imaging technology in our study, we resorted to immunofluorescence staining for the analysis of cell migration. This approach provided quantitative migration data, including cell counts across various regions and the morphology of cells within the migrating areas. These data are instrumental in comparing the migration efficacy of cells on fibrous membranes under various parameters and serve as a foundation for the preliminary validation of the regulatory impact of cell adhesion to scaffolds on SCs migration. For further construction and research of the scaffold in future, we plan to use advanced live-cell workstations and live-cell time-lapse imaging technology to more accurately demonstrate the regulatory effect of the scaffold on cellular behavior.

In addition to spherical particles such as SiO_2, hybrid fibers incorporating nanorods, nanotubes, and irregularly shaped particles have been investigated.[27] Despite the diversity in their fabrication techniques, the majority of these hybrid fibers were produced using composite electrospinning methods. Consequently, the shape, size, and spatial distribution of the particles, as well as the morphology of the protrusions they form on the fibers, are potential determinants of cellular behavior. Taking spherical, isotropic particles like SiO_2 as an example, using anisotropic particles such as nanorods can generate asymmetric surface protrusions, which may alter the dynamics of focal adhesions (such as the involvement of neurite filopodia in neurons), thereby affecting the migration of neural cells. Irregularly shaped particles may lead to uneven surface roughness, which could influence the process of cell migration and the growth of neurites. As an illustrative example, the extensional state of mouse fibroblasts in poly(lactic-*co*-glycolic acid (PLGA)) fibers doped with halloysite nanotubes (HNTs) and carbon nanotubes (CNTs) was found to vary with the concentration of particles. On fibers containing 5% HNTs, the cells exhibited longer extension, which may be attributed to the topological cues provided by the tubular particles.[28] According to the relevant literature, the incorporation of CNTs in PVA/chitosan (CS) fibers enhances cell adhesion and proliferation, attributed to the improved protein adsorption capacity of the CNTs.[29] Analogously, this mechanism may also be applicable to

elucidating the impact of non-spherical particles on cellular migration, suggesting that irregular surfaces may offer a greater number of protein binding sites, facilitating the formation of a biochemical microenvironment conducive to cell migration.

Upon comprehensive analysis, the 200 nm 6% treatment group demonstrated the most effective regulation of SC migration across all experimental groups. Furthermore, the compatibility test outcomes for the nanofibers engineered with SiO_2 protrusions, as depicted in Fig. S6 (ESI†), showed no statistically significant differences among the groups except for the 200 nm, 1% group, 200 nm, 3% group, PCL group, and Con group. Although the statistical findings suggest variations between the groups, the specific values of cellular activity are found to be virtually identical among them. This finding suggests that nanofibers featuring SiO_2 protrusions possess excellent biocompatibility and are not toxic to cells. Following this, we conducted investigations into the regulatory influence of "cell climbing stones" with varying parameters on cellular migration, utilizing NSCs that are proficient at self-renewal and multilineage differentiation.[30–34]

The NSCs, which had been continuously cultured for a period of four to six days and had formed into cell spheres, were seeded onto nanofibers that featured SiO_2 protrusions as secondary structures of varying diameters and concentrations. Following a further five days of culture, the outward migration of NSCs from the core of the cell spheres was monitored. This was conducted to assess the regulatory impact of the "cell climbing stones" with protrusions exhibiting different parametric characteristics on the migration of NSCs. Fig. 3 and 4 illustrate the fluorescence images depicting the outward migration of NSCs from the center of the cell spheres and present statistical analysis of their migration distances. NSCs from all groups exhibited outward migration from their central location. Specifically, the NSCs in the Con group were observed to migrate outward radially from the center.

In contrast, NSCs cultured on nanofibers with distinct protrusion parameters displayed a directional migration pattern. Guided by topographical cues, these cells were able to discern the surrounding microenvironment and actively select migration paths. As a result, the oriented nanofiber arrays were

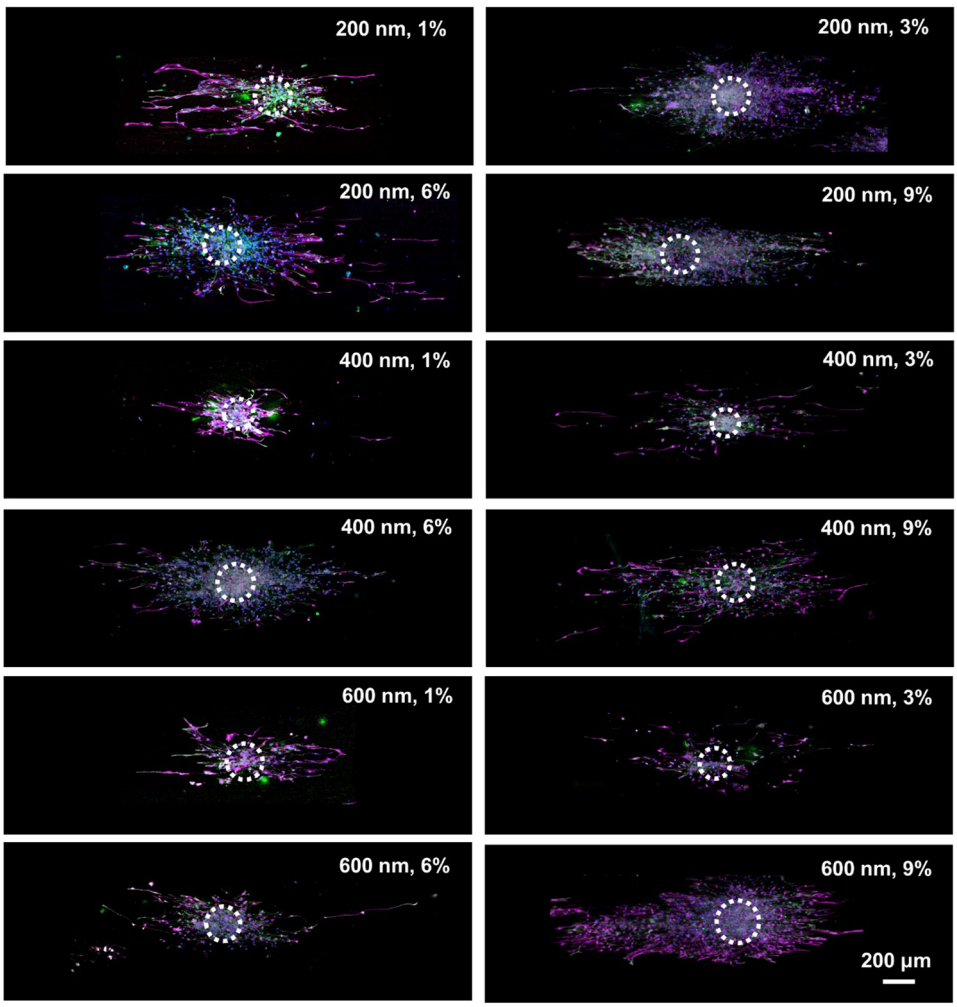

Fig. 3 Fluorescence images of the migration of NSCs from the NSC spheres after culture for 5 days on the different PCL/SiO_2 nanofibers. Purple: MAP-2; Green: GFAP; Blue: DAPI.

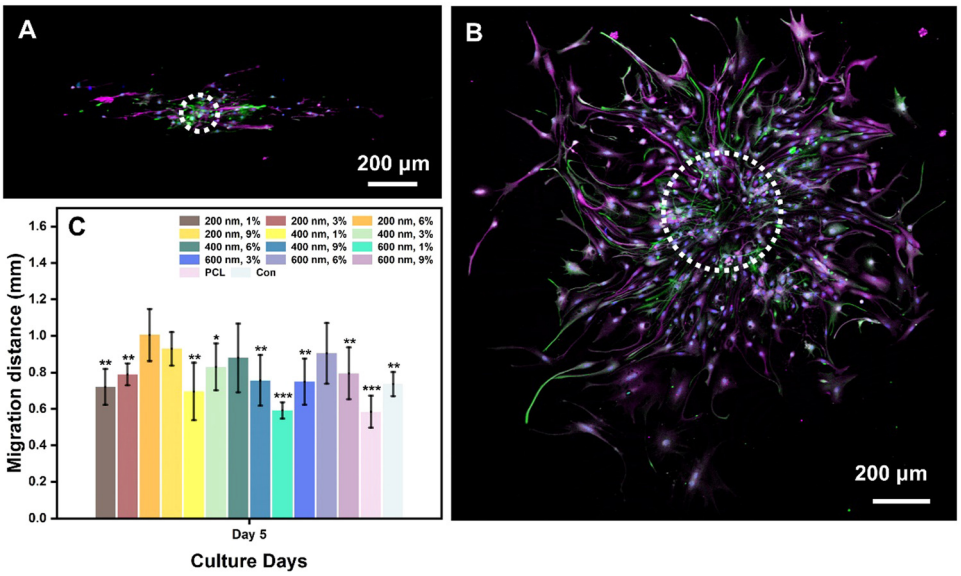

Fig. 4 (A, B) Fluorescence images of the migration of NSCs from the NSC spheres after culture for 5 days on (A) group PCL and (B) group Con. Purple: MAP-2; Green: GFAP; Blue: DAPI. (C) Maximum migration distance of NSCs on the different samples. *$P < 0.05$, and **$P < 0.01$ as compared with group 200 nm, 6%.

successful in orchestrating NSCs migration from the core of the cell aggregates towards the periphery. Fig. 4C summarizes the average maximum distance of NSCs migration from the center of cell spheres. The 200 nm, 6% group, 200 nm, 9% group, 400 nm, 6% group, and 600 nm, 6% group all exhibited very impressive migration distances, with statistically significant differences compared to the other groups. Among them, the 200 nm 6% group showed the most significant migration distance, with a maximum distance reaching 1.239 mm.

An increase in the SiO_2 content within the fibers leads to a decrease in the inter-particle distance between adjacent SiO_2 grains. This reduction in spacing facilitates the narrowing of the intervals between contact signals. Sufficiently spaced intervals are conducive to the perception by the cells of topographical cues. Consequently, following the detection of short-range structural cues, the cells undergo morphological alterations. Upon sensing topological features, they exhibit an increased frequency of exploration and deformation. During the process of cellular migration, the initial attachment and subsequent elongation of the cell's leading edge are contingent upon the contact guidance offered by the underlying extracellular matrix. This is followed by focal adhesion formation at the trailing edge of the migrating cell. This suggests that the orientation of SiO_2 protrusions and the arrangement of fibers exert a significant influence on migration dynamics.[1,21,35] Furthermore, for the migration of NSCs, a parameter of 200 at a 6% concentration has been found to optimally regulate their migratory behavior. Excluding the influence of SiO_2 particle diameter, it is evident that at a concentration of 6% for SiO_2 protrusions, NSCs exhibit a consistently superior migration distance. Additionally, analysis of Fig. 3 and 4 reveals that NSCs begin differentiating into neurons (as indicated by MAP-2 staining) while migrating outward from the core. Consequently, the question of whether the PCL/SiO_2 hybrid fibers with surface protrusions can concurrently enhance the growth of axons in pre-differentiated neurons is the next critical aspect of our investigation that requires exploration.

We examined the influence of "cell climbing stones" featuring surface protrusions with distinct parameters on neurite outgrowth in neurons. The fluorescence microscopy images depicted in Fig. 5A and B illustrate the neurite outgrowth of neurons following 7 d and 14 d of culture on uniaxially aligned PCL/SiO_2 hybrid fibers and decorated with 200 nm protrusions of various concentrations. The average neurite lengths and the maximum neurite lengths for neurons in each group are presented in Fig. 5C and D. For the 200 nm protrusions, after 7 d of culture, the average neuron axon length in the 6% group was the longest, specifically 54.24 ± 18.09 μm, and there were significant differences between this group and the others. Following a 14-day cultivation period, a considerable increase in the length of neurons was observed across all groups. The 200 nm, 6% group and the 200 nm, 3% group displayed average neurite lengths measuring 100.14 ± 57.87 μm and 95.77 ± 61.26 μm, respectively. No statistically significant difference was detected between these two groups. However, both exhibited statistically significant differences compared to the neurite lengths of neurons in the other groups. The longest neurite for each group is depicted in Fig. 5D. On both the 7th and the 14th day of cultivation, the maximum length of neurites was observed in the 200 nm, 6% group. It is evident that by the 14th day, there has been a discernible increase in the length of neuronal neurites. Upon a comprehensive analysis of the data from all groups and a comparison with the pure PCL group (Fig. 5B), it is noted that the neuronal neurites did not grow uniformly in the direction of the aligned nanofibers. Instead, they tended to extend in a more disorganized pattern. In this

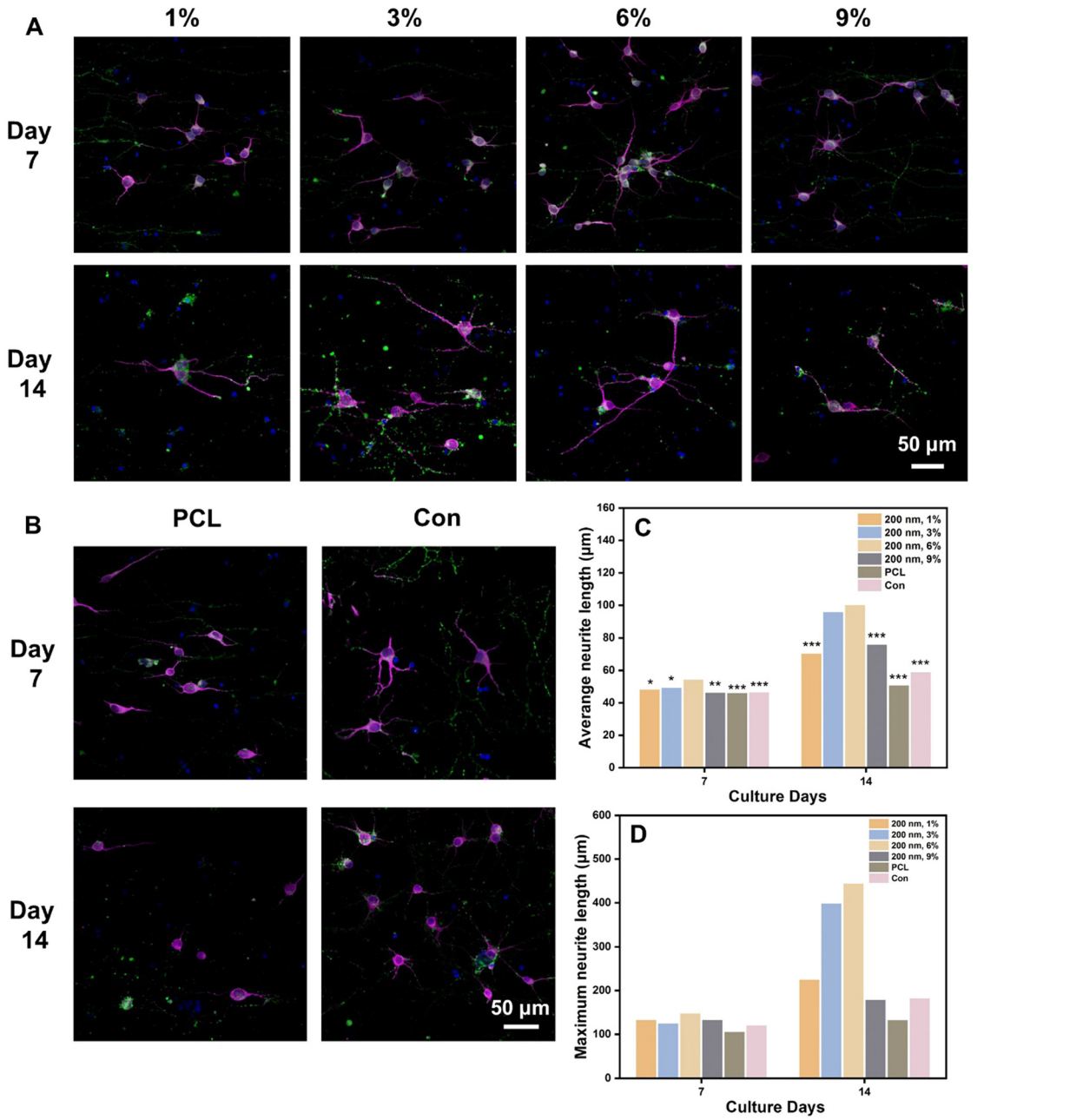

Fig. 5 (A, B) Fluorescence images of the neurite outgrowth from neurons on the different fibers after culture for 7 and 14 days: (A) group 200 nm, 1%, 3%, 6% and 9%; (B) group PCL and Con. Purple: MAP-2; Green: SYP; Blue: DAPI. (C) The average and (D) maximum neurite length of the neurons cultured on group 200 nm. *$P < 0.05$, **$P < 0.01$, and ***$P < 0.001$ as compared with group 200 nm, 6%.

context, we hypothesize that this is due to the presence of protuberances on the hybrid fiber surface, which provide attachment points for neurons between the parallel fibers, allowing them to grow across the two fibers without adhering to the direction of the aligned fibers.

Similarly, we examined the growth of neuronal neurites on PCL/SiO_2 hybrid fibers with protrusion diameters of 400 nm and 600 nm after culturing for 7 d and 14 d. As depicted in Fig. S7 and S8 (ESI†), for fibers with a 400 nm protrusion diameter, following a 7 d culture period, the average neuronal axon lengths in the 400 nm, 3% group and 400 nm, 6% group were observed to be the longest, exhibiting statistically significant differences compared to the other groups. However, upon reaching the 14th day, the neurons in the 400 nm, 1% group exhibited the longest average neurite length (Fig. S8A, ESI†). Notably, as shown in Fig. S8B (ESI†), the longest neurites observed at days 7 and 14 were associated with the 400 nm, 6% group and 400 nm, 9% group, respectively. Consequently, a direct summary of the relationship between the growth of neuronal neurite length and the dimensions of the protrusions, as well as concentration, is not readily apparent. Similarly, Fig. S7A (ESI†) shows the morphologies of neurons on hybridized

nanofibers after 7 d and 14 d of culture, and when the SiO_2 diameter is 400 nm, the neurites of the neurons still do not extend in accordance with the direction of the nanofibers. Upon culturing neurons with hybrid nanofibers having SiO_2 protrusions of 600 nm, the 600 nm, 6% group and 600 nm, 9% group exhibited the longest average neurite length after 7 d of culture. Following a 14-day culture period, no statistically significant variations were observed in neurite length across different hybridized fiber types within any of the groups (Fig. S8C, ESI†). Notably, the neurite lengths in these groups were found to be significantly greater than those in neurons derived from the pure PCL and Con groups. Fig. S7B (ESI†) depicts the morphology of neurons cultured on hybrid nanofibers after 7 d and 14 d in culture. In comparison to the 200 nm and 400 nm tip sizes, neurons displayed an improved orientation of axonal growth when the SiO_2 tip diameter was 600 nm. This enhancement in axonal orientation is presumably attributed to the mismatch between the larger tip size and the dimensions of neuronal filopodia, which facilitates stronger topographical guidance from the aligned nanofibers, thereby allowing neurons to extend their neurites along the direction of the fiber alignment.

Neuronal growth cones are capable of detecting physical and biochemical signals that originate from the extracellular matrix or the surrounding environment. The incorporation of SiO_2 nanoparticles contributes to the creation of nanoscale sensing platforms for neurite elongation, thereby enhancing the process of neurite growth. Concurrently, radially arranged nanofibers facilitate tissue regeneration by promoting cellular migration and enhancing neurite extension, which holds significant promise for applications in the closure and repair of augmenting neurite elongation and cellular migration synergistically. Building upon the structure of radially aligned nanofibers, the introduction of appropriate secondary structures on their surface, such as nanoscale protrusions, can serve to deliver contact cues and mimic the trajectory of radially aligned axonal pathways. Future integration with bioactive signals is anticipated to synergistically augment neurite elongation and cellular migration.

The introduction outlined that the dimensions of filopodia on neural cell growth cones typically range from 100 to 300 nm. Our experimental results indicate that protrusions of 200 nm had a pronounced regulatory impact on neural cells, outperforming those with larger diameters of 400 nm and 600 nm. This observation suggests that the size of the protrusions may serve as an optimal anchoring point for filopodia, akin to the fit between climbing holds and a climber's hand. Consequently, the size of nanoscale protrusions could be a pivotal factor in modulating neural cell behavior.

Maintaining a consistent protrusion size, the concentration of SiO_2 was found to modulate the density of signals by adjusting the spacing between protrusions. For protrusions measuring 200 nm, an optimal spacing was achieved at an SiO_2 concentration of 6%, which provided the cells with continuous guidance cues. This resulted in optimal cell migration and neurite outgrowth in the 200 nm, 6% group. Notably, for SiO_2 protrusions of different sizes, the concentration that most effectively regulates cell behavior varies. Currently, we can only confirm that the 200 nm, 6% combination yields the most favorable outcome. Thus, both the size and concentration of SiO_2 are critical determinants in the regulation of cell behavior, with complex interplay between the two factors. Further investigation, including molecular biology techniques like Western blotting, is needed to clarify the relative importance of each factor.

3. Conclusions

By utilizing a simplified electrospinning process, we integrated SiO_2 nanoparticles, produced using the Stöber synthesis, with biocompatible PCL to fabricate hybrid nanofibers featuring surface protrusions as secondary structures with distinct sizes and SiO_2 concentrations. The resulting structure mimics a "rock wall" and is hence termed a "cell climbing stone." We explored the regulatory influence of "cell climbing stone" constructs with different parameters on the migration of SCs, NSCs, and the growth of neuronal neurites. Our investigation revealed that nanofibers featuring oriented protrusions significantly enhance the motility of SCs and NSCs, as well as facilitating the extension of neuronal neurites. Comparative analysis of a range of parameters revealed that nanofibers composed of SiO_2 NPs with a diameter of 200 nm, when combined with PCL to achieve a SiO_2 concentration of 6%, demonstrated the most pronounced influence on the behavior of neural cells. The "cell climbing stone" architecture, developed within this study, shows promise for application in the design of multi-layered neural conduits. The nanofibers exhibiting optimal dimensions (200 nm in diameter and 6% SiO_2 concentration) are proposed to function as the inner layer of these conduits, facilitating directional topological guidance for cellular migration and axonal regeneration. Furthermore, the surface protrusions on these nanofibers are expected to interact synergistically with bioactive agents, such as nerve growth factor (NGF), to further enhance the migration of neural cells and the extension of axons. Additionally, the substitution of SiO_2 within the cell climbing stone with mesoporous SiO_2 is anticipated to enable the controlled release of signaling molecules, thereby synergistically augmenting the regeneration and repair processes of neural tissues.

Author contributions

Yawen Wang: data curation, formal analysis, methodology, validation, writing – original draft. Xiaopei Zhang: data curation, methodology. Lijie Yao: formal analysis, investigation. Yuying Yan: investigation, methodology. Yuanfei Wang: Supervision, writing – review & editing. Tong Wu: conceptualization, funding acquisition, methodology, supervision, writing – review & editing.

Conflicts of interest

The authors declare that they have no known competing financial interests or personal relationships that could have appeared to influence the work reported in this paper.

Data availability

Data are available upon request from the authors.

Acknowledgements

This research was supported by Natural Science Foundation of Shandong Province (ZR2024JQ026), National Natural Science Foundation of China (32171322, 12411530081), Special Funds for Taishan Scholars Project of Shandong Province (No. tsqn202211125).

References

1 X. Zhang, M. Guo, Q. Guo, N. Liu, Y. Wang and T. Wu, *Mater. Today Adv.*, 2023, **17**, 100343.
2 N. Liu, X. Ning, X. Zhang, Z. Zhou, M. Fu, Y. Wang and T. Wu, *Adv. Technol. Neurosci.*, 2024, **1**, 276–289.
3 X. Zhao, X. Lu, K. Li, S. Song, Z. Luo, C. Zheng, C. Yang, X. Wang, L. Wang, Y. Tang, C. Wang and J. Liu, *Bioact. Mater.*, 2023, **24**, 331–345.
4 J. Xue, T. Wu, J. Li, C. Zhu and Y. Xia, *Angew. Chem., Int. Ed.*, 2019, **58**, 3948–3951.
5 W. Hällström, T. Mårtensson, C. Prinz, P. Gustavsson, L. Montelius, L. Samuelson and M. Kanje, *Nano Lett.*, 2007, **7**, 2960–2965.
6 V. Brunetti, G. Maiorano, L. Rizzello, B. Sorce, S. Sabella, R. Cingolani and P. P. Pompa, *Proc. Natl. Acad. Sci. U. S. A.*, 2010, **107**, 6264–6269.
7 D. Y. Fozdar, J. Y. Lee, C. E. Schmidt and S. Chen, *Biofabrication*, 2010, **2**, 035005.
8 A. Ferrari, M. Cecchini, A. Dhawan, S. Micera, I. Tonazzini, R. Stabile, D. Pisignano and F. Beltram, *Nano Lett.*, 2011, **11**, 505–511.
9 N. Gomez, Y. Lu, S. Chen and C. E. Schmidt, *Biomaterials*, 2007, **28**, 271–284.
10 J. Xie, W. Liu, M. R. MacEwan, P. C. Bridgman and Y. Xia, *ACS Nano*, 2014, **8**, 1878–1885.
11 J. Xue, T. Wu, J. Qiu, S. Rutledge, M. L. Tanes and Y. Xia, *Adv. Funct. Mater.*, 2020, **30**, 2002031.
12 S. Fan, L. Qi, J. Li, D. Pan, Y. Zhang, R. Li, C. Zhang, D. Wu, P. Lau, Y. Hu, G. Bi, W. Ding and J. Chu, *Adv. Healthcare Mater.*, 2021, **10**, 2100094.
13 X. Ma, M. Xiao, Y. Hao and G. Cheng, *Carbon*, 2019, **145**, 90–99.
14 S. H. Lee, H. B. Lee, Y. Kim, J. R. Jeong, M. H. Lee and K. Kang, *Nano Lett.*, 2018, **18**, 7421–7427.
15 J. He, C. Sun, Z. Gu, Y. Yang, M. Gu, C. Xue, Z. Xie, H. Ren, Y. Wang, Y. Liu, M. Liu, F. Ding, K. W. Leong and X. Gu, *ACS Nano*, 2018, **12**, 9660–9668.
16 L. He, Z. Sun, J. Li, R. Zhu, B. Niu, K. L. Tam, Q. Xiao, J. Li, W. Wang, C. Y. Tsui, V. W. Hong Lee, K.-F. So, Y. Xu, S. Ramakrishna, Q. Zhou and K. Chiu, *Biomaterials*, 2021, **268**, 120585.
17 A. Omidinia-Anarkoli, J. W. Ephraim, R. Rimal and L. De Laporte, *Acta Biomater.*, 2020, **113**, 350–359.
18 T. Wu, J. Xue and Y. Xia, *Angew. Chem., Int. Ed.*, 2020, **59**, 15626–15632.
19 P. K. Mattila and P. Lappalainen, *Nat. Rev. Mol. Cell Biol.*, 2008, **9**, 446–454.
20 K. Kang, S. Y. Yoon, S.-E. Choi, M.-H. Kim, M. Park, Y. Nam, J. S. Lee and I. S. Choi, *Angew. Chem., Int. Ed.*, 2014, **53**, 6075–6079.
21 Y. Liu, X. Zhang, Y. Wang, M. Guo, J. Sheng, Y. Wang and T. Wu, *Chem. Commun.*, 2023, **59**, 10753–10756.
22 Y. Jin, D. Yang, D. Kang and X. Jiang, *Langmuir*, 2009, **26**, 1186–1190.
23 B. B. Patel, F. Sharifi, D. P. Stroud, R. Montazami, N. N. Hashemi and D. S. Sakaguchi, *Macromol. Biosci.*, 2019, **19**, 1800236.
24 C. M. M. Motta, K. J. Endres, C. Wesdemiotis, R. K. Willits and M. L. Becker, *Biomaterials*, 2019, **218**, 119335.
25 R. Mayor and S. Etienne-Manneville, *Nat. Rev. Mol. Cell Biol.*, 2016, **17**, 97–109.
26 Q. Liu, S. Zheng, K. Ye, J. He, Y. Shen, S. Cui, J. Huang, Y. Gu and J. Ding, *Biomaterials*, 2020, **263**, 120327.
27 W. Huang, Y. Xiao and X. Shi, *Adv. Fiber Mater.*, 2019, **1**, 32–45.
28 R. Qi, M. Shen, X. Cao, R. Guo, X. Tian, J. Yu and X. Shi, *Analyst*, 2011, **136**, 2897–2903.
29 H. Liao, R. Qi, M. Shen, X. Cao, R. Guo, Y. Zhang and X. Shi, *Colloids Surf., B*, 2011, **84**, 528–535.
30 R.-S. Hsu, P.-Y. Chen, J.-H. Fang, Y.-Y. Chen, C.-W. Chang, Y.-J. Lu and S.-H. Hu, *Adv. Sci.*, 2019, **6**, 1900520.
31 B. Zhang, W. Yan, Y. Zhu, W. Yang, W. Le, B. Chen, R. Zhu and L. Cheng, *Adv. Mater.*, 2018, **30**, 1705694.
32 G. Martino, S. Pluchino, L. Bonfanti and M. Schwartz, *Physiol. Rev.*, 2011, **91**, 1281–1304.
33 E. Scott-Solomon and R. Kuruvilla, *Dev. Cell*, 2020, **53**, 691–705.e697.
34 B. L. Wise, M. F. Seidel and N. E. Lane, *Nat. Rev. Rheumatol.*, 2021, **17**, 34–46.
35 J. He, Q. Liu, S. Zheng, R. Shen, X. Wang, J. Gao, Q. Wang, J. Huang and J. Ding, *ACS Appl. Mater. Interfaces*, 2021, **13**, 42344–42356.